Interpretation of Light Curves of IP Peg in a Model with Shockless Interaction between the Gas Stream and Disk

T. S. Khruzina[1], A. M. Cherepashchuk[1], D. V. Bisikalo[2], A. A. Boyarchuk[2], and O. A. Kuznetsov[3]

[1]*Sternberg Astronomical Institute, Universitetskiĭ pr. 13, Moscow, 119899 Russia*
[2]*Institute of Astronomy, Russian Academy of Sciences, ul. Pyatnitskaya 48, Moscow, 109017 Russia*
[3]*Keldysh Institute of Applied Mathematics, Russian Academy of Sciences, Miusskaya pl. 4, Moscow, 125047 Russia*
Received December 8, 2000

Abstract—We have analyzed light curves of the eclipsing cataclysmic variable IP Peg. A model with a shockless interaction between the gaseous stream and disk (i.e., an elliptical disk with a "hot line") can describe the main characteristic features of the light curve of the interacting close binary better than a classical model with a "hot spot" at the outer boundary of a circular accretion disk. In particular, the hot-line model can reproduce the luminosity increase observed at phases $\varphi \sim 0.1$–0.2 and $\varphi \sim 0.5$–0.6, which is not possible in the standard hot-spot model. The advantages of the hot-line model are particularly striking for the IR light curves of IP Peg: the discrepancy χ^2 between the theoretical and observed light curves is 49 for the model with a shockless interaction between the gaseous stream and disk, and 2681 for the standard hot-spot model. © *2001 MAIK "Nauka/Interperiodica".*

1. INTRODUCTION

A three-dimensional gas-dynamical model of the gas flows in interacting close binary systems (CBSs) was considered in [1–3]. These calculations showed that, in the steady-state case, a gaseous stream flowing from the inner Lagrange point (L_1) and the accretion disk form a structure with a single morphology, since the point of tangency between the stream and disk is free of discontinuities and shocks, so that a classical "hot spot" cannot be formed [4, 5]. At the same time, the interaction between the gaseous stream and the intercomponent envelope of the CBS forms an extended shock wave along the edge of the stream: a "hot line" [1–3, 6]. This shock can explain the characteristic features of the light curves of cataclysmic variables [7], in particular, the occurrence of both regular and anomalous humps accompanying eclipses of the accretion disk by the donor star.

Here, we present the results of applying new procedures for light-curve synthesis [8] developed on the basis of three-dimensional gas-dynamical calculations [1–3, 7]. Unlike [7], we consider a more realistic model with an elliptical accretion disk with an extended bright region (hot line) along the stream emerging from L_1. Using IP Peg, a cataclysmic variable with a double eclipse, as an example, we have derived model parameters from the mean light curve. Models with an elliptical disk and hot line can fit the main features of the light curves of the interacting CBS better than classical models with a hot spot at the outer boundary of a circular accretion disk.

2. PHYSICAL JUSTIFICATION OF THE MODEL

Mass transfer between the components in a semi-detached binary is traditionally described according to the following scheme: (a) gas flows from the donor star through the inner Lagrange point L_1 and forms a stream; (b) stream material with excess angular momentum is unable to be accreted directly and forms a gaseous ring around the accretor; (c) this gaseous ring spreads out under the action of dissipative processes in the accretion disk, and some fraction of this material falls onto the surface of the accretor.

In the late 1960s, Gorbatskiĭ [4] and Smak [5] suggested that the interaction between the stream and accretion disk is accompanied by the formation of a shock wave, and a hot spot forms at the point of contact between the stream and disk. Over the last thirty years, this model has been widely applied in studies of cataclysmic binaries (see, for example, [9]), and has been used to explain the presence of humps in light curves, although many observational properties of these systems have remained beyond its scope.

In recent years, gas-dynamical models for the mass transfer in semi-detached CBSs have been radically revised [1–3, 7]. Three-dimensional gas-dynamical calculations [1–3, 6] have shown that, in a steady-state flow regime, the gaseous stream and accretion disk undergo a shockless interaction, and do not form a classical hot spot. These calculations indicate that the stream–disk system has a single morphology, and that the transition from the stream to the disk is free of dis-
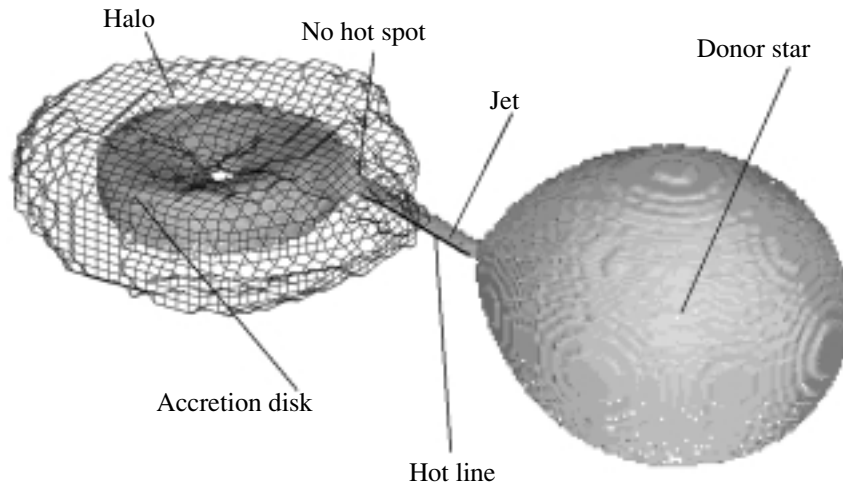
Fig. 1. The structure of mass transfer in a CBS. The white spot in the center of the disk indicates the location of the accretor.

continuities and shocks. In addition, the flow pattern in CBSs is substantially more complicated than implied by the above simple scheme. In addition to the stream and accretion disk, a gaseous "halo" forms around the accretion disk and intercomponent envelope of the system. The gas of the intercomponent envelope flows around the accretor and collides with the stream from L_1, forming a shock front along the edge of the stream (the hot line). Figure 1 presents a schematic of the basic elements of the calculated flow structure for the cataclysmic binary IP Peg: the density iso-surface at the $\rho = 10^{-3}\rho(L_1)$ level and the contours of the halo corresponding to $\rho = 10^{-4}\rho(L_1)$.

Models for mass transfer in CBSs with a hot line instead of a hot spot are fairly universal. Variations of the viscosity, radiative energy-loss rate, and other conditions of the gas flows in CBSs [10–12] do not qualitatively affect the basic conclusion of the three-dimensional gas-dynamical calculations: in a steady-state mass-transfer regime, classical models with a hot spot, usually considered to be the region where the gaseous stream collides by the outer boundary of the disk, must be replaced by models with a hot line formed outside the disk, along the gaseous stream, due to the interaction of the stream with the intercomponent envelope. It was shown in [7] that the hot line can adequately explain the presence of humps in CBS light curves.

To study the structure of the disk and circum-disk formations during outbursts, we should observe systems with highly inclined orbital planes, in which the eclipse of the accretion disk by the secondary star can be seen. We have chosen the CBS IP Peg, which has a so-called double eclipse; i.e., at the moment of lower conjunction of the donor star, this star consecutively eclipses not only the white dwarf, but also the asymmetrical accretion structure surrounding it. The classical model can describe the double-eclipse profile rea-

sonably well; however, it cannot reproduce some parts of the curves outside of eclipse, especially at epochs of outburst, when an anomalous hump appears in the light curve.

3. MATHEMATICAL MODEL OF THE SYSTEM

The hot-line model is in better agreement with the observations than the hot-spot model [7], but also needs refinement. Comparison of synthetic and observed light curves will enable the determination of a number of parameters, which can then be used to improve gas-dynamical models for mass transfer in semi-detached binaries. A detailed gas-dynamical model and correct mathematical representation via a photometric model will open fresh opportunities for analysis of the rich observational data available for interacting CBSs. It will also make it possible to determine more accurately the physical characteristics and evolutionary statuses of different types of interacting CBSs. This is particularly important in the context of prospects for the launch of UV satellite observatories (for example, SPECTR-UV), which will provide opportunities for detailed observations of interactions between gaseous structures in CBSs. Here, we use a simplified blackbody hot-line model.

The mathematical model used to synthesize the theoretical light curves and estimate the parameters of the interacting CBS [8] is based on the three-dimensional structure of the gaseous flows in these systems suggested by the results of [1–3, 10–12]. The basic assumptions of the photometric model can be formulated as follows.

(1) The donor star (secondary) fills its Roche lobe entirely; i.e. we take into account both its tidal and rotational deformation.

(2) The surface of the donor star is divided into 648 area elements. For each, the radiation intensity directed toward the observer is calculated taking into

account gravitational darkening, limb darkening, and the effect of heating by radiation from the white dwarf. For each phase, we consider only areas facing the observer, taking into account their eclipse by all components of the system, including the donor star.

(3) The white dwarf (primary) is spherical and located at one focus of the elliptical accretion disk. The surface of the white dwarf is also divided into 648 area elements. The effective temperature of these areas is assumed to be the same over the entire surface of the star. We take into account limb darkening when calculating the radiation intensity directed toward the observer. Areas on the white dwarf can be eclipsed by the body of the star itself, the accretion disk, the donor star, and the hot line.

(4) The figure of the elliptical accretion disk is determined as follows [8]: (a) the lateral (outer) surface of the disk is specified by an ellipsoid with semi-axes a, b and c, with a and b in the orbital plane and $b^2 = a^2(1 - e^2)$, and with c perpendicular to the orbital plane; (b) the center of the white dwarf is located at one focus of the ellipsoid; (c) the inner surfaces of the disk result from subtracting from the ellipsoid those sections of the ellipsoid that fall on the inner regions of two paraboloids, specified by the parameter A_p.

The axes of the paraboloids determining the inner disk surface are perpendicular to the orbital plane. The parameter A_p depends on the angle of rotation ψ of the radius vector from the vertex of the paraboloid to the edge of the disk about the paraboloid axis. At the disk periastron, $\psi = 0$, and $\psi = \pi$ at apoastron. The coefficient $A_p(\psi)$ is

$$A_p(\psi) = \frac{Ab^2}{a^2(1 + e\cos\psi)} = \frac{A(1 - e^2)}{1 + e\cos\psi}, \qquad (1)$$

where A is constant. For $e = 0$, this coincides with the paraboloid constant A_{par} [13] describing the shape of the inner surfaces of a circular disk, $A_p(\psi) = A = \text{const}$. In the case of an elliptical disk, we obtain $A_p(\psi) = A(1 - e)$ at periastron ($\psi = 0$), and $A_p(\psi) = A(1 + e)$ at apoastron ($\psi = \pi$). The vertices of the paraboloids are shifted relative to the orbital plane of the CBS by $z_0 = \dfrac{R_w^2}{A^2(1 - e)^2}$: these are below and above the orbital plane for the upper and lower paraboloids, respectively. For this choice of z_0 with $\psi = 0.0$ (at disk periastron), the paraboloids will intersect the orbital plane at a distance R_w from the white dwarf's center, where R_w is the radius of the white dwarf. We assumed that the inner (for example, upper) surface of the disk is formed by that part of the paraboloid with non-negative z coordinates. The lines of intersection of the ellipsoid describing the lateral part of the disk and the paraboloids describing its inner parts specify the upper and lower disk boundaries. These are located a distance h from the orbital plane:

$$h = \pm c\left(\sqrt{\frac{c^2 A^4}{4b^4} - \frac{1}{b^2}\left[\frac{R_w^2}{(1 - e)^2} - a^2\right]} - \frac{cA^2}{2b^2}\right). \qquad (2)$$

The orientation of the disk is specified by the angle α_e between the radius vector from the white dwarf's center to the disk periastron and the line connecting the CBS components. α_e can vary from 0 to 2π, and increases in the direction of the orbital motion of the components. A detailed description of modeling of a geometrically thick elliptical accretion disk is presented in [13].

When calculating the temperature of an area element on the disk surface, we took into account the dependence on the distance r between the center of the element and the white-dwarf surface. The temperatures of areas on the disk near the white-dwarf surface were taken to be equal to the temperature T_{bw} of the surface layer located near the equator of the star, with $T_{bw} \geq T_w$. In [8, 13], the temperatures of areas on the disk were specified by the temperature of the white dwarf T_w. However, observations indicate that, in many cataclysmic variables, the temperature of the inner part of the disk substantially exceeds T_w. In addition, the observed radiation flux from the white dwarf is relatively small, and is not able to provide the observed heating of the secondary. The heating of the disk is associated with the transformation of the gravitational energy of matter into heat in the course of its motion toward the surface of the white dwarf. It is generally assumed that the disk surface temperature T_g varies with distance from the center of the white dwarf r according to the law

$$T_g = T_{bw}\left(\frac{R_w}{r}\right)^{\beta_g}. \qquad (3)$$

To first approximation, the parameter β_g is usually taken to be $\beta_g = 3/4$ [14], assuming that each point of the disk surface radiates as a blackbody. In reality, however, the radial temperature distribution turns out to be flatter than a 3/4 law, especially during outbursts. Apart from the above relation, the temperature of a disk area element can increase by several percent due to heating by radiation from the white dwarf and secondary.

(5) The hot line along the stream is described by a section of an ellipsoid with semi-axes a_v, b_v and c_v extended toward the inner Lagrange point L_1 (Fig. 2). The lateral surface of this ellipsoid coincides with the tangent line to the elliptical disk independent of its orientation, while its center is located in the orbital plane inside the disk at some distance from its edge. Figure 2 presents a schematic of the basic CBS elements used in the photometric model for an orbital inclination $i = 0°$ (the view from above). The arrows in the graphs indicate the direction of gas motion in the disk. A detailed

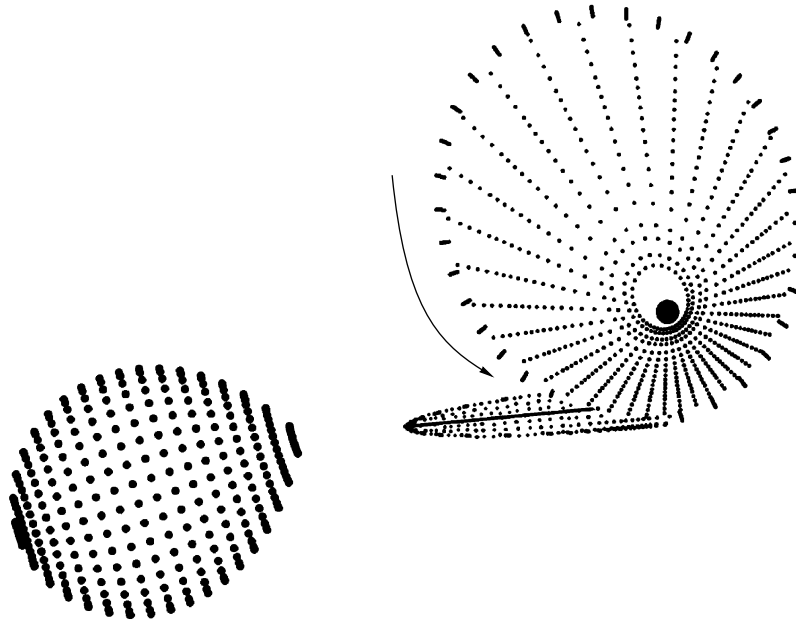**Fig. 2.** Schematic of the basic elements of a CBS in the photometric model at orbital phase $\varphi = 0.8$, for orbital inclination $i = 0°$ (view of the system from above). The arrow indicates the direction of gas motion in the disk. The thick curve marks a conventional boundary between the windward and leeward sides of the hot line.

description of the construction of the figure of the hot line and synthesis of the CBS light curve is given in [8].

De-excitation of the shock at the surface of the hot line can occur both at the shock front, i.e., on the side of the incident flow (which we will call the "windward" side), and on the opposite ("leeward") side, depending on the physical parameters and optical depths of the interacting streams (their velocity, density, etc.). In Fig. 2, the thick curve indicates a conventional boundary between the windward and leeward sides of the hot line at the surface of the truncated ellipsoid. Our photometric model assumes that areas on the hot-line surface emit blackbody radiation. This assumption is valid only when the optical depth of the hot line exceeds unity. The temperature of the ith area element on the hot-line surface is calculated separately for each of its sides in accordance with the following relation adopted in the model:

$$T_i(y) = T_{min} + T_{max} \cos\left(\frac{\pi}{2}\Delta y_i\right), \tag{4}$$

where y is the coordinate along the major axis of the hot-line ellipsoid, and

$$\Delta y_i = \frac{y_i - y_{max}}{y_{min} - y_{max}}. \tag{5}$$

For the adopted temperature law, the temperature increment reaches its maximum ($T_i(y) = T_{min} + T_{max}$) at the point with coordinate y_{max}, and is equal to zero ($T_i(y) = T_{min}$) at the point with coordinate y_{min}. We take

the minimum temperature to be the temperature of matter a distance r from the white-dwarf center, according to the temperature distribution (3). If y_{min} and y_{max} are close to each other, the shock is de-excited within a small region similar to a classical hot spot, but this region is located on the hot line rather than on the disk. The rest of the hot line remains relatively cool ($T \sim 1500$–2000 K). Figure 3 presents the temperature distribution along the major axis of the hot-line ellipsoid from the windward (curve 1) and leeward (curve 2) sides. The D indicates the y coordinate of the point of tangency of the hot-line ellipsoid and the lateral surface of the accretion disk, and P indicates the y coordinate of the pole of this ellipsoid. Unlike the case considered in [8], our model supposes that the maximum temperature on the windward side of the hot line T_{max} is reached at the point of tangency of the stream and the lateral disk surface (in [8], $y_{max}^{(1)}$ was a free parameter). The maximum temperature of the hot line on the leeward side is shifted toward the point with y coordinate

$$y_{max}^{(2)} = y_{max}^{(1)} - dy, \tag{6}$$

with the displacement dy being a free parameter. Despite the fact that the temperature on the windward side of the hot line is higher than it is on the leeward side, the radiating area there is half that on the leeward side. In addition, the contribution of the windward side of the hot line to the total flux from the system depends not only on the temperature contrast at the surface of the truncated ellipsoid, but also on the position of the
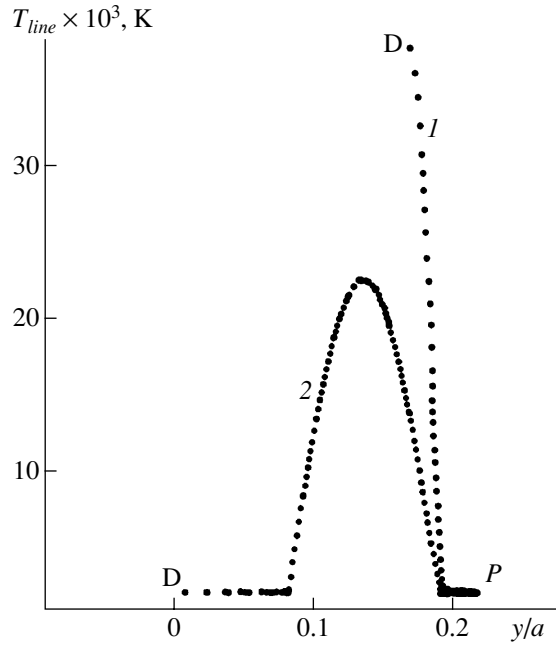
Fig. 3. Temperature distribution along the major axis *Y* of the ellipsoid describing the hot line on the windward (curve *1*) and leeward sides (curve *2*). The D indicates the *y* coordinates of points of tangency between the body of the hot line and the lateral surface of the disk; the *P* indicates the *y* coordinate of the pole of the ellipsoid describing the hot line. The maximum temperature is $T_{max}^{(1)} = 35370$ K on the windward side of the line and $T_{max}^{(2)} = 22400$ K on the leeward. The parameters of the de-excitation region are $a_v = 0.088a_0$, $b_v = 0.217a_0$, $c_v = 0.014a_0$, $y_{min} = 0.19a_0$, and $dy = 0.033a_0$. Other parameters of the CBS correspond to Case 2 from Table 1.

disk and the compactness of the de-excitation zone. The hottest areas on the windward side of the hot line may be obscured from the observer by the lateral surface of the disk or by the donor star.

(6) The parameters of the problem are: the mass ratio of the components $q = M_w/M_2$ (M_w and M_2 are the masses of the white dwarf and donor star); the orbital inclination of the system *i*; the effective temperature of the donor star T_2, without taking into account heating by hot radiation of the white dwarf; the radius and effective temperature of the white dwarf R_w and T_w; the temperature T_{bw} of the surface layer at the equator of the white dwarf, where the accretion occurs; the parameters *e*, *a*, *A*, α_e describing the size, shape, and orientation of the elliptical disk; and, finally, parameters describing the shape of the hot line (a_v, b_v, c_v), the temperature distribution at its surface y_{min} and dy [see (5)], and the temperature itself T_{max} on both the windward and leeward sides. Thus, in general, the number of unknown parameters reaches 17. In our study, we use the classical temperature distribution along the disk radius 3/4 [14]; otherwise we would have another free

parameter. Therefore, it makes sense to try to use the hot-line model to determine the parameters of CBSs whose basic parameters *q*, *i*, T_2, T_w, R_w, *a*, and *A* have independent estimates from other sources.

To estimate the adequacy of the fit of an observed light curve, we calculate the residual

$$\chi^2 = \sum_{j=1}^{n} \frac{(m_j^{theor} - m_j^{obs})^2}{\sigma_j^2}, \qquad (7)$$

where m_j^{theor} and m_j^{obs} are the theoretical and observed stellar magnitudes at orbital phase *j*, σ_j^2 is the dispersion of the observations at point *j*, and *n* is the number of points in the curve.

We estimate the model parameters from the CBS light curve using the Nelder–Meade method to minimize the residual functional χ^2 [15]. The solution of the problem or corresponding confidence interval for the obtained parameters is usually taken to be represented by the set of parameters for which the residual is lower than some critical significance level of the distribution $\chi_{\eta, N}^2$. Here, η is the chosen probability for rejecting a correct solution and *N* is the number of normal points in the light curve. If none of the resulting solutions has a residual below the chosen significance level $\chi_{\eta, N}^2$, the effect of varying a particular parameter can be estimated by specifying some arbitrary limiting residual instead of the critical residual—for example, by increasing the minimum residual by about 10%.

A detailed description of the light-curve synthesis, the method used to determine the parameters of the problem, and the results of some model calculations are presented in [8].

4. THE IP Peg SYSTEM

Dwarf novae are a subclass of cataclysmic variables with short outbursts lasting several days, during which the luminosity of the system increases by 3^m–5^m. The outbursts may recur after several weeks or several years, depending on the type of the system.

Variability of IP Peg was detected by Lipovetskiĭ and Stepanyan [16]. Goranskij *et al.* [17] demonstrated that the system is an eclipsing dwarf nova with period $P = 3^h.8$ displaying sharp and deep eclipses, as well as a pronounced orbital hump in its light curve. During its outbursts, which recur with an interval of ~100 days, the brightness of IP Peg increases by approximately $2^m.5$, and its out-of-eclipse *V* magnitude varies from $14^m.7$ in the inactive state (outside eclipse) to ~$12^m.3$ during outburst.

The results of photometric observations of IP Peg are presented in [18–23] and of spectral observations in [24–27]. In the recent spectral observations [28, 29],

Balmer line emission was detected, which comes from the polar regions of the donor star and is the result of heating by the hot radiation of the white dwarf. These spectral observations also provide some evidence that spiral waves can exist in the accretion disk during outbursts in the system.

The presence of the secondary is manifest in the ellipsoidal variability, which can clearly be seen in the infrared. Szkody and Mateo [18] estimated the orbital inclination $i \sim 75°$ and distance $d \sim 130–142$ pc of the system from the K-band light curve. According to the color indices, the spectral type of the secondary is M4V. The mass–radius relation indicates that the star is near the main sequence.

Based on the duration of the ingress and egress of eclipses of the components of the IP Peg system by the red dwarf derived from high-speed photometric observations during the main minimum, Wood and Crawford [19] estimated the component mass ratio to be $2.04 < q < 2.86$ and the orbital inclination to be $80°.9 < i < 90°$. Their preferred value was $q \simeq 2.04$ for $i \simeq 80°.9$.

Based on H_β and H_γ observations of the system in the inactive stage, Marsh [24] determined the half-amplitudes of the radial velocity curves for the components to be $K_w = 173 \pm 17$ km/s for the white dwarf and $K_2 = 301 \pm 19$ km/s for the secondary (from absorption lines). In the determination of K_2, possible shifts of the centers of absorption lines due to heating of the donor star by radiation from the inner regions of the disk were taken into account. As a result, the component mass ratio was somewhat lower than that obtained by Wood and Crawford [19]: $q \simeq 1.67 \pm 0.1$. The orbital inclination was estimated to be $i = 79° \pm 0°.9$, the distance between the components to be $a_0/R_\odot = 1.50 \pm 0.08$, and the mass and radii of the components to be $M_w/M_\odot = 1.14 \pm 0.15$, $M_2/M_\odot = 0.67 \pm 0.12$, $R_w/R_\odot = 0.0058 \pm 0.0021$, and $R_2/R_\odot = 0.498 \pm 0.032$. The estimated temperature of the white dwarf was $T_w \leq 15\,000$ K, based on the flux variations during the egress of the star from eclipse. Martin *et al.* [26] obtained $K_2 = 298 \pm 8$ km/s for the half-amplitude of the radial velocity curve of the secondary, based on observations of He I line emission within a few days of outburst. They also derived component parameters close to those obtained by Marsh [24]: $q = 1.70 \pm 0.11$, $i > 68°$, $K_2 = 298 \pm 8$ km/s, $M_w/M_\odot = 1.15 \pm 0.10$, $M_2/M_\odot = 0.67 \pm 0.08$, and $R_2/R_\odot = 0.502 \pm 0.024$.

Wolf *et al.* [21] detected appreciable variations of the disk radius during outburst. Prior to the outburst, the radius was rather small ($R_d \sim 0.24a_0$); it increased to $\sim 0.37a_0$ on the descending branch after the outburst maximum, and then gradually fell to $\sim 0.26a_0$. After a second outburst, the disk radius again increased to $\sim 0.34a_0$, and then decreased to $\sim 0.28a_0$ after several days. Analysis of the temperature distribution along the disk radius during the outburst indicated that the temperature profile was rather flat, and only on the edge of

the disk did it correspond to a "3/4" law. In the inactive state, the temperature variations were close to a classical "3/4" law. The disk temperature during the outburst was ~ 8000 K in inner regions and ~ 4500 K at the edge [23]. The IR (1.45–1.85 μm) observations of the system in its inactive state of Froning *et al.* [30] showed that the bulk of the disk has a flat surface-brightness distribution and low brightness temperature (~ 3000 K). The disk radius suggested by the IR observations is $R_d \sim 0.32a_0$.

The light curve of the system has a pronounced pre-eclipse hump with amplitude $\Delta B \sim 1^m$ [17], which begins near orbital phase $\varphi \sim 0.65$ and reaches its maximum at phases $\varphi \sim 0.8–0.9$. This hump is usually interpreted as the radiation of a hot spot at the boundary of the disk. It is considerably less pronounced in lines than in the continuum. The emission-line light curve displays a nearly *V*-shaped eclipse of the accretion disk by the secondary. The average temperature of a classical hot spot is $11\,000–13\,000$ K [24]. Szkody [32] obtained a high blackbody temperature of $\sim 20\,000$ K for the spot from IUE spectra. For a spot temperature $T_{sp} = 12\,000$ K, the vertical size of the hot spot is roughly double the thickness of the outer edge of the disk. The maximum of the hump falls at phase $\varphi \sim 0.85$, which means that the shock front is not perpendicular to either the gas flow (the predicted maximum is located at phase $\varphi \sim 0.78$) or the disk ($\varphi \sim 0.95$), but instead is located somewhere between these values. Along with the regular orbital hump, Wolf *et al.* [33] detected a second hump in the light curve near phase $\varphi \sim 0.4$ in the inactive state of the system, with an amplitude half that of the first hump, which they explained as radiation of the hot spot above the upper edge of the disk. The azimuth of the hot spot in the IR differs both from that specified by the theoretical path of the gaseous flow and from that in the optical [30].

High-time-resolution spectroscopy of IP Peg indicated the presence of a large-scale bright azimuthal structure in the outer parts of the disk during outburst [27, 29, 35–38]. Doppler tomography of IP Peg suggests that these formations are the same as the spiral waves in the accretion disk discovered by Sawada *et al.* [34]. Note that spectra obtained at the end of outburst or in the inactive state do not display spiral waves. Morales-Rueda *et al.* [38] detected a large-scale asymmetry in the system during an outburst, roughly on the line connecting the components, along with the spiral structure in the disk. The asymmetry is manifest in a shift of emission-line eclipses by 0.015–0.045 of the orbital period to phases earlier than the white dwarf eclipse. The hot-line region between the system components may well prove to be this asymmetrical structure.

5. THE *V*-BAND LIGHT CURVE OF IP PEG

5.1. The Hot-Line Model for the Inactive State of IP Peg

To demonstrate the adequacy of the hot-line model for the IP Peg system in its inactive state, we used the light
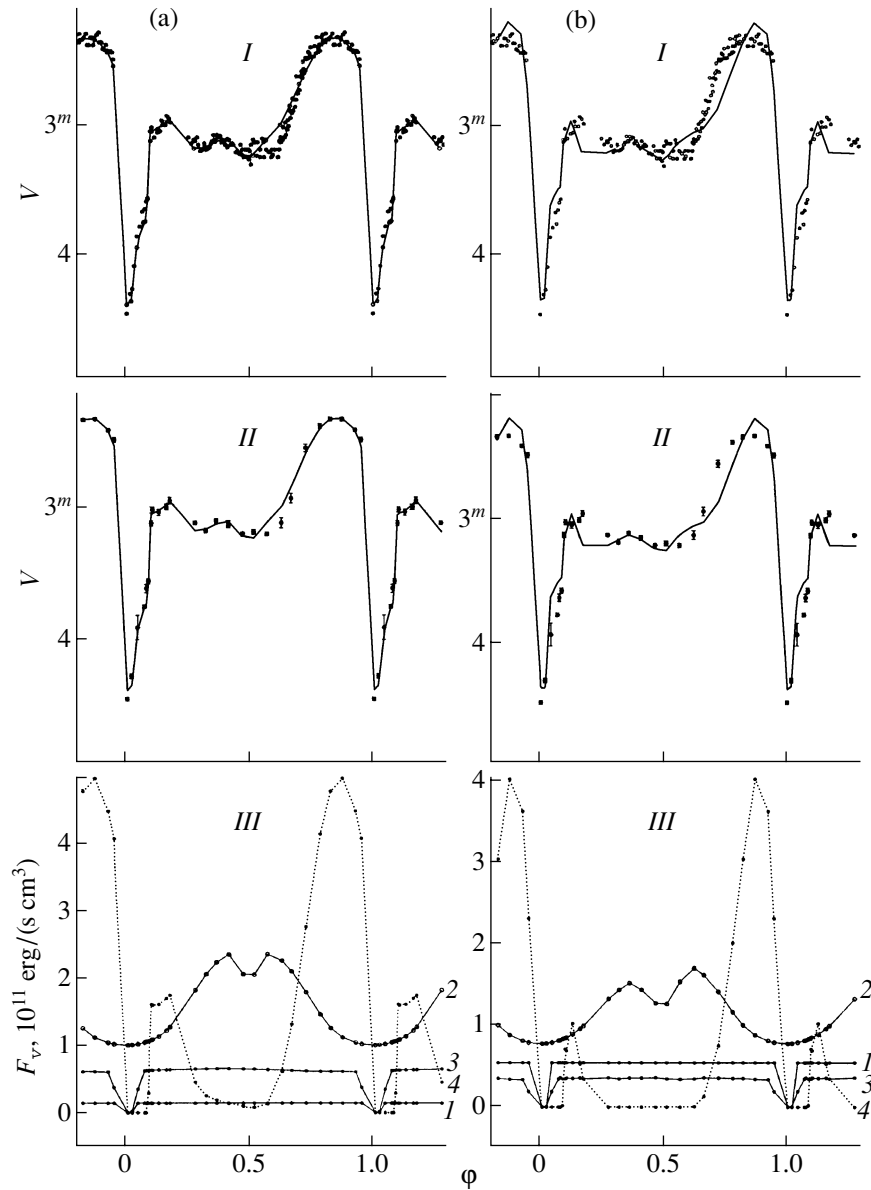
Fig. 4. IP Peg (*I*) observations and (*II*) mean light curve in the *V* filter in the inactive state. The solid curves indicate light curves synthesized with the best-fit parameters (Table 1, "case 1") for the (a) hot-line model and (b) the classical hot-spot model. The graphs *III* present the contribution of the system's components to the total radiation: (*1*) the white dwarf, (*2*) donor star, (*3*) disk, and (*4*) area of energy release (for (a) a hot line or (b) hot spot).

curve of IP Peg in the *V* band obtained during an international coordinated campaign to observe dwarf novae [22]. The light curve combines observations for three nights from December 6 to 26, 1988 corresponding to the inactive state of the system (a regular outburst was detected five days after the latest observation), and provides fairly good coverage of the orbital period [Fig. 4 (plots *I*, *II*)].

The mean light curve is represented by 26 normal points. The critical significance level for $\eta = 0.001$ and number of degrees of freedom $N = 26$ was $\chi^2_{0.001, 26} = 54.1$.

When estimating the parameters of IP Peg, the intervals of variation for some of them (q, i, R_w, T_w, T_2, a)

were restricted using values derived from observations in other studies. Table 1 presents these intervals and the values obtained for the other parameters. In Fig. 4a (graph *I*), the points indicate observations of IP Peg, and the solid curve marks the theoretical light curve synthesized with the parameters given in Table 1 ("case 1"). The theoretical curve fits the observations of the system in the main minimum very well; the time of egress from the white-dwarf eclipse and the amplitude of the brightness jump are approximated well, as is the anomalous hump near $\varphi \sim 0.4$. The fit for out-of-eclipse observations near orbital phases $\varphi \sim 0.6$–0.75 is somewhat worse: the discrepancy between the theoretical

Table 1. Parameters of IP Peg (from *V* observations)

Parameter	Generally accepted value	Classical model (I)	Hot-line model (II) inactive state case 1	Hot-line model (II) inactive state case 2	active state
$q = M_w/M_2$	1.56–2.86	2.47	1.707	1.714	1.708
i, deg	78–90	85.4	80.15	80.45	80.11
R_w/a_0	0.0023–0.0056	0.0052	0.0061	0.0061	0.0062
R_2/a_0	0.295–0.373	0.316	0.344	0.344	0.344
T_w, K	≤15000	45965	16009	16188	16200
T_{bw}, K	40000–50000	45965	43246	40300	70045
T_2, K	3100–3400	3397	3424	3403	3445
Disk					
a/a_0	0.24–0.28	0.407	0.308	0.256	
a/a_0 (active)	~0.34–0.37				0.463
z/a	~0.02–0.04	0.031	0.041	0.039	
z/a (active)	~0.2				0.137
Model I: Spot					
Azimuth, deg	18–79	24.5			
R_{sp}/a_0		0.198			
T_{sp}, K	~12000–20000	4530			
Model II					
e		0	0.315	0.251	0.142
α_e, deg			43.8	271	57.4
a_v/a_0			0.041	0.088	0.112
b_v/a_0			0.204	0.217	0.178
c_v/a_0			0.019	0.014	0.098
$\langle T^{(1)} \rangle$, K			17146	13500	–
$T_{max}^{(1)}$, K			21637	35370	–
$\langle T^{(2)} \rangle$, K			10872	12120	5723
$T_{max}^{(2)}$, K			21618	20405	6180
χ^2		1199	172	231	1210

Model I is the classical hot-spot model [39], Model II is the hot-line model [8]. The large residual obtained for the light curve in the active state is due to the low rms errors of the normal points.

and observed curves reaches $\Delta m = 0\overset{m}{.}1$. We can see from Fig. 4a (graph *III*), which presents the relative contributions of the system components to the total flux, that the shape and amplitude of the hump at phases $\varphi \sim 0.6$–0.9 is determined primarily by the radiation of the hot line. The white dwarf's contribution is insignificant, mainly due to the small size of the star. The accretion disk is rather cool: the temperature of its inner regions does not exceed 10000–15000 K, and the temperature at the outer edge is $T \sim 2200$–2700 K. The disk has appreciable eccentricity, $e \sim 0.13$, and its orientation is $\alpha_e \sim 44°$. The temperature distribution over the hot-line surface indicates that the areas of energy

release are rather compact on both the windward and leeward sides. The temperature of the hot line in the zone of energy release exceeds the disk temperature in adjacent regions by a factor of ~ten. At the maximum, this temperature increases to ~24100 K on the windward side in the shock region, and to ~23400 K on the leeward side. The average hot-line temperatures are ~17150 K and ~10900 K, respectively. The surface of the truncated ellipsoid describing the shape of the hot line is cool near its *y* pole; its temperature is comparable to that of the outer parts of the disk (~2200 K). Note that this is one of a series of solution obtained with approximately the same goodness of fit, but over a

broader interval of possible values for q, i, R_w, T_w, T_2, and a. We have chosen this solution because it is in agreement with the results of spectral studies.

The minimum residual for the solution $\chi^2 = 172$ exceeds the critical value $\chi^2_{0.001, 26} = 54.1$. Note that, in our photometric model, neither the radiation of the stream from L_1 nor that of the circumstellar envelope was taken into account. Also, a set of simplifying assumptions was used. Therefore, the excess of the solution residual over the critical value is natural. To estimate the impact of various parameters on the solution, we used a limit for the residual $\chi^2 = 189$ rather than the critical limit, thereby increasing the minimum residual by 10%. For most of the parameters, the allowed intervals of their variation were within 1–2% of their best-fit values. For the maximum temperatures of the hot line on the windward and leeward sides, the resulting errors are 7.5 and 2.8%, respectively; we have for the parameter dy $\Delta dy \sim 10\%$, and also $\Delta e \sim 3\%$, $\Delta a_v \sim 5.2\%$, $\Delta q \sim 4.8\%$, and $\Delta \alpha_e \sim 12\%$ of the best-fit values for the set of parameters used.

Table 1 ("case 2") contains another solution for the light curve of IP Peg in its inactive state. Here, the eccentricity of the disk is somewhat higher than in the previous case, $e \sim 0.25$, and the orientation $\alpha_e \sim 270°$. This model is characterized by an appreciable difference between the temperatures of the hot line on the windward and leeward sides (Fig. 3): at the maximum, it increases to ~ 37000 K (± 4000 K) on the windward side, and to ~ 22000 K (± 700 K) on the leeward side. The amplitude of the corresponding temperature variation is indicated in parentheses, for an increase of the residual by 10% (to $\chi^2 = 254$) and for the best-fit values of the other parameters. The average hot-line temperatures are ~ 13500 and ~ 12120 K, respectively. Figure 5 presents the theoretical light curve and the contributions of the components to the total radiation flux.

5.2. The Classical Hot-Spot Model

When a classical model with a circular disk and a hot spot [39] is used to interpret the IP Peg V-band light curve, the consistency between the theoretical curve and the observations becomes appreciably worse [Table 1, Fig. 4b (graphs *I*, *II*)]. We have not been able to adequately fit the out-of-eclipse brightness of the system: at phases $\varphi \sim 0.15$–0.35 and $\varphi \sim 0.65$–0.95, the discrepancy between the theoretical and observed curves reaches $\Delta m = 0.^{m}25$. In addition, the main minimum with the double eclipse is also fit substantially worse than it is with the hot-line model: at phases $\varphi \sim 0.08$–0.12, the discrepancy between the theoretical and observed curves reaches $\Delta m = 0.^{m}2$. In the classical model, the amplitude and shape of the hump at phases $\varphi \sim 0.6$–0.9 are also specified primarily by the radiation of a rather extended hot spot (Fig. 4b, graph *III*) with radius

$\sim 0.2a_0$. The contribution of the disk and white dwarf to the total radiation flux remain insignificant. The contribution of the radiation from the outflowing component is somewhat asymmetrical about orbital phase $\varphi = 0.5$, due to our allowance for heating of the surface of the donor star by the high-temperature radiation of the hot spot (this heating is asymmetrical about the line connecting the centers of mass of the stars). The classical model requires a supplementary source of radiation to provide the broader hump at phases $\varphi \sim 0.6$–0.9, which cannot be fit with a single hot spot. Thus, the hot-line model is preferable to the classical model as a description of IP Peg's light curve in its inactive state.

5.3. The Hot-Line Model for the Active State of IP Peg

The hot-line model was initially proposed for steady-state flow regimes in CBSs. In outburst, the flows in IP Peg are undoubtedly not steady, so that non-steady-state gas-dynamical models should be used to analyze the light curve in the active state. Nevertheless, we attempted to analyze the light curve of IP Peg at an outburst maximum using the hot-line model. The resulting solution may be useful for determining the domain of applicability for the hot-line model.

We used the V-band light curve of IP Peg obtained by Webb *et al.* [31] (Fig. 6) on September 28, 1997 (curve No. 4558) at the very maximum of an outburst. The out-of-eclipse brightness of the system increased by almost a factor of 7.5 (by $2.^{m}2$) compared to the inactive state of the system. The curve is represented by 28 normal points with errors from $0.^{m}01$–$0.^{m}02$ for out-of-eclipse brightness to $0.^{m}07$ at the minimum of the curve. For this light curve, we appreciably restricted the allowed values for the parameters $q = 1.707 \pm 0.002$, $i = 80°.1 \pm 0°.3$, $R_w/a_0 = 0.0061 \pm 0.0001$, $T_2 = 3424 \pm 30$ K, and $T_w = 16009 \pm 200$ K to the indicated limits. The remaining parameters were varied freely. In addition, we introduced a supplementary free parameter: the power-law index β_g in dependence (3). We assumed that this index may differ from the classical value 3/4 during outburst. This is required by the fact that increasing the disk radius alone during the outburst, even from the inactive-state value $a \sim 0.63 R_{L1}$ to the boundary of the critical Roche lobe, is unable to yield the observed increase of the V flux. The spectral data indicate that the radiation intensity from the area of energy release (either the hot spot or hot line) varies only little. A fairly good agreement between the theoretical and observed light curves was reached for $\beta_g = 0.6$.

The sixth column of Table 1 contains the resulting parameters of the system; Figs. 6a and 6b present the theoretical curve constructed using these parameters. The out-of-eclipse flux of the system (Fig. 6c) is $F_V \sim 3.2 a_0^2$ erg s^{-1} cm^{-3}, which is a factor of ~ 4.6 higher than at the maximum of the orbital hump in the inactive
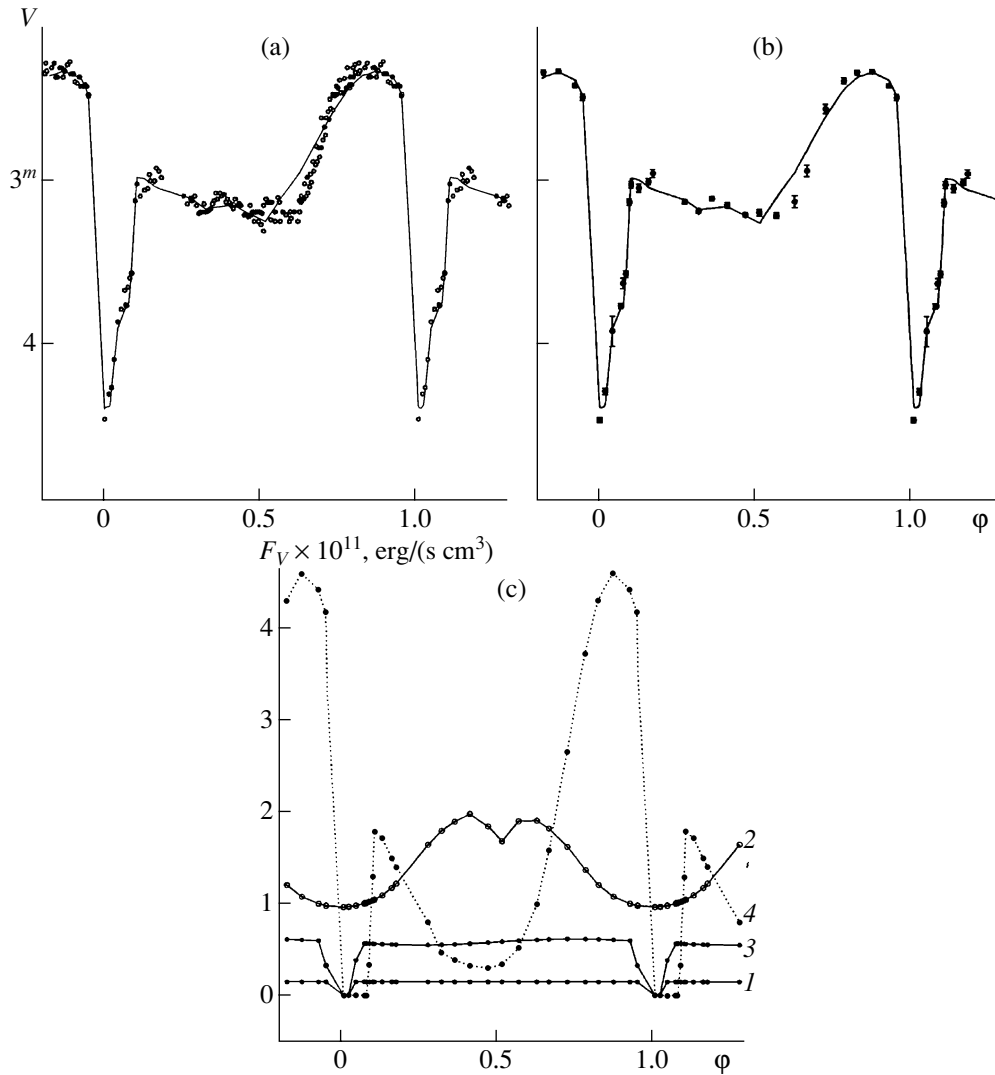
Fig. 5. IP Peg (a) observations and (b) the mean light curve in the *V* filter in the inactive state. The solid curves indicate light curves synthesized with the best-fit parameters (Table 1, "case 2") for the hot line model; (c) contributions of the system's components to the total radiation: (*1*) the white dwarf, (*2*) donor star, (*3*) disk, and (*4*) hot line.

state (Fig. 4c). The low value of the *V* flux (40% lower than observed) may be due to the fact that this model neglects additional sources of radiation, such as the radiation of spiral waves in the accretion disk. Their contribution is no less than ~15% of the total luminosity of the disk, and the temperature in the spiral regions reaches 20000 K [35]. The presence of spiral waves during outburst could also be responsible for the fluctuations of the out-of-eclipse flux (Figs. 6a, 6b). A more complicated model describing the "spiral" distribution of the temperature over the disk is required to test this hypothesis. It is also possible that this discrepancy reflects the non-Planckian character of the radiation from the gaseous structures in CBSs. In this connection, we stress once again that our CBS model can only be used to calculate relative flux variations. The calculation of absolute fluxes and colors requires that the real

spectra of gaseous structures in CBS be taken into account, which we plan to do in future studies.

It is notable that, with the parameters used, the hot line model essentially coincides with the classical hot-spot model. With the given size and orientation of the truncated ellipsoid describing the hot line, we obtain only a modest bulge on the lateral surface of the disk instead of a line. The windward side of the hot line is entirely submerged in the disk, and radiation is observed only from the leeward side. This is probably a result of the non-steady-state character of the flow during outburst. The hot-line model is only valid for a steady-flow regime. During outburst, the collision of the expanding disk with the stream results in the formation of a shocked region analogous to a hot spot. The observations appear to be consistent with this picture.
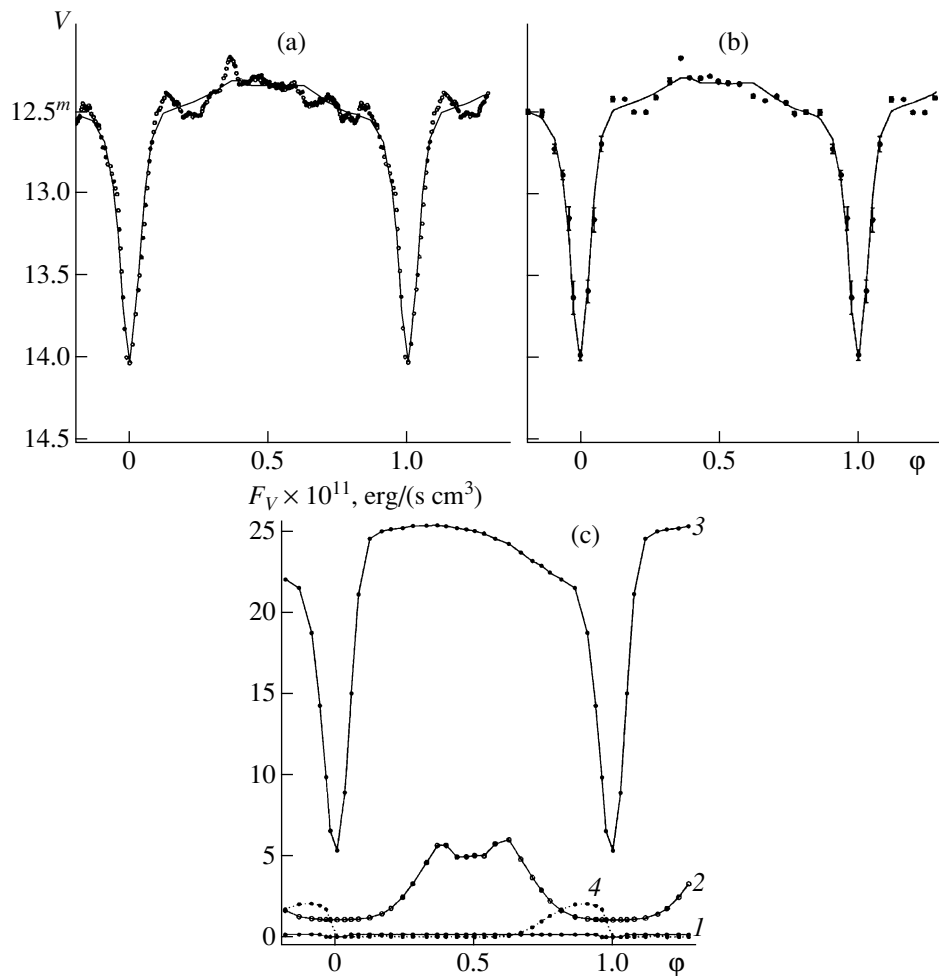
Fig. 6. IP Peg (a) observations and (b) mean light curve in the *V* filter in the maximum of a burst. Solid lines indicate light curves synthesized with the best-fit parameters (Table 1) within the "hot line" model; (c) the contribution from the system components to its total radiation: from the (*1*) white dwarf, (*2*) the donor star, (*3*) the disk and (*4*) the energy release area.

6. THE INFRARED LIGHT CURVE OF IP Peg

The advantages of the CBS model taking into account the extended shock in the region of the collision between the gaseous stream and the matter flowing around the accretion disk were most obvious when we considered the IR light curve of the IP Peg system in its inactive state. We studied the light curve of IP Peg obtained by Froning *et al.* [30] on September 28–30, 1994 in the *H* filter ($\lambda = 1.45$–1.85 μm). The nearest outbursts were observed on October 25, 1993 and December 7, 1994. The shape of the light curve was essentially the same on all nights, which enabled combination of all observations into a single curve (Fig. 7a). Attempts to fit this curve using only the ellipsoidal variations of the secondary and a fairly broad range of possible parameter values were unsuccessful [30]. There is apparently a supplementary source of radiation in the system, with intensity comparable to that of a red dwarf at IR wavelengths. This source varies dramatically with orbital phase. It can be neither the accretion disk,

whose contribution does not exceed 8% of the total flux (according to various estimates), nor a classical hot spot, which can be observed only in a narrow interval of orbital phases. It is even less likely to be the white dwarf, whose contribution in the IR is negligibly small.

The results of our interpretation of the IP Peg light curve in the *H* filter in both a classical hot-spot model and a hot-line model are presented in Table 2. Analyzing the light curve in the hot-line model, we restricted the allowed intervals for the parameters $q = 1.707 \pm 0.003$, $i = 80°\!.1 \pm 0°\!.5$, $R_w/a_0 = 0.0061 \pm 0.0001$, $T_2 = 3420 \pm 50$ K, and $T_w = 16000 \pm 350$ K within the indicated limits, as was done for the *V*-band light curve during outburst. The remaining parameters were varied freely, including the power-law index β_g in (3). Figures 7a and 7b present the observed light curves and the theoretical curves synthesized using the parameters from Table 2. This figure indicates excellent agreement between the curves: both the amplitudes of the bright-
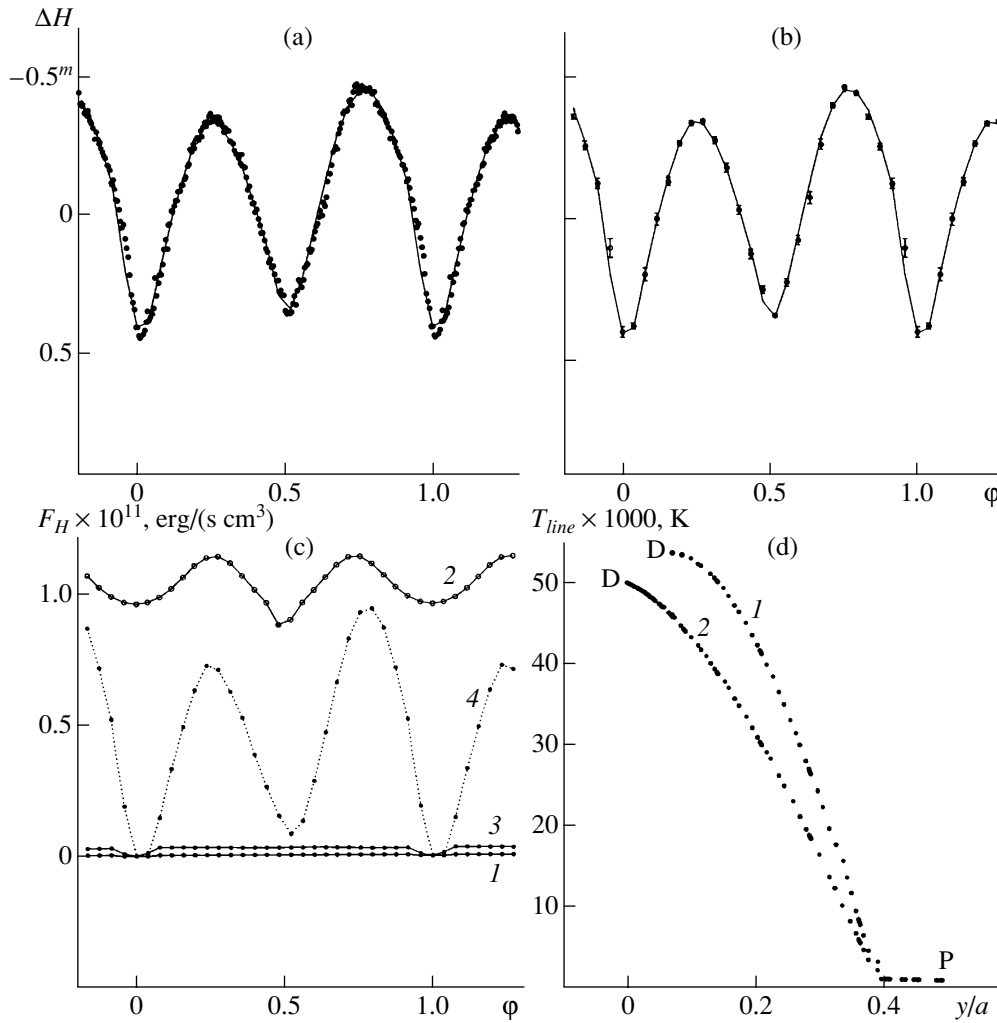
Fig. 7. IP Peg (a) observations and (b) mean light curve in the H filter in the inactive state. The solid curves indicate light curves synthesized with the best-fit parameters (Table 2) for the hot-line model; (c) contribution of the system's components to its total radiation: (1) the white dwarf, (2) donor star, (3) disk, and (4) hot line; (d) temperature distribution along the major axis Y of the ellipsoid describing the hot line on the windward (curve 1) and leeward (curve 2) sides, obtained from the analysis of the IP Peg light curve in the inactive state. The maximum temperature is $T_{\max}^{(1)} = 50720$ K on the windward side of the line and $T_{\max}^{(2)} = 48100$ K on the leeward side. The parameters of the de-excitation region are $a_v = 0.018a_0$, $b_v = 0.502a_0$, $c_v = 0.014a_0$, $y_{\min} = 0.39a_0$, and $dy = 0.13a_0$.

ness maxima and the depths and widths of the minima are well fit.

The size of the accretion disk (more exactly, of the part that is optically thick in the near-IR) is small: $R_d/a_0 \sim 0.12$–0.22 ($a/a_0 \simeq 0.17$, $e \simeq 0.29$). Its contribution to the total flux is 1.5–2%; its out-of-eclipse flux is essentially constant and does not appreciably affect the light-curve shape. The radial temperature dependence of the disk, indeed, deviates from the "3/4" law (we find from the solution $\beta_g = 0.69$); however, due to the small contribution of the disk radiation to the total flux, this should not be considered a firm conclusion. The brightness temperature of the inner part of the disk reaches 9000–13 000 K; the brightness temperature in the outer

regions of the optically thick region of the disk decreases to 2000–3000 K.

As expected, the largest contribution to the total flux (~60% in quadrature) comes from the red dwarf, whose polar region is heated by hot radiation from the boundary layer of the white dwarf (Fig. 7c). The parameters of the donor star (mass, radius, and temperature) correspond to the values we obtained from the V-band light curve. More unexpected is the rather substantial contribution of the hot line to the near-IR light curve. Both the windward and leeward sides of the hot line are required to explain the residual radiation obtained by Froning *et al.* [30] after removing the ellipsoidal variability of the donor star from the light curve. The brightness temperature of the hot line (Fig. 7d) at the $\tau \sim 1$ level

Table 2. Parameters of IP Peg (in the inactive state) from *H* observations

Parameter	Generally accepted values	Classical model (I)	Hot-line model (II)
$q = M_w/M_2$	1.56–2.86	2.146	1.705
i, deg	78–90	80.33	80.34
R_w/a_0	0.0023–0.0056	0.0063	0.0061
R_2/a_0	0.295–0.373	0.325	0.344
T_w, K	≤15000	38145	16349
T_{bw}, K	40000–50000	38145	23620
T_2, K	3100–3400	3477	3468
Disk			
a/a_0	~0.33	0.57	0.17
z/a	~0.02–0.04	0.028	0.0047
β_g	≤0.75	0.75	0.69
Model I: Spot			
Azimuth, deg	~60	80	
R_{sp}/a_0	0.1–0.15	0.144	
T_{sp}, K	~10000	17130	
Model IU			
e			0.288
α_e			66.6
a_v/a_0			0.018
b_v/a_0			0.502
c_v/a_0			0.014
$\langle T^{(1)} \rangle$, K			27880
$T^{(1)}_{max}$, K			50720
$\langle T^{(2)} \rangle$, K			25300
$T^{(2)}_{max}$, K			48100
χ^2		2681	49

reaches 54000 K on the windward and 50000 K on the leeward side; the opaque part of the line is fairly narrow and extended. This can explain the substantial flux of the *H* radiation at orbital phases $\varphi \sim 0.1$–0.4, and this is precisely the part of the orbital light curve that cannot be fit with the classical hot-spot model.

When we compare the calculated model parameters in the visible (Table 1) and IR (Table 2), it is clear that they are in good agreement, given that the analyzed light curves were obtained at different times and probably at different phases of activity of the system. The only parameter that changes appreciably is the temperature of the hot line, which roughly doubles in the transition from optical to IR wavelengths. This may be due to the deviation of the hot-line radiation from a black-body law. If we suppose that bremsstrahlung and recombination radiation contribute significantly to the total radiation of the hot line, an increase in the brightness temperature in the transition toward longer wavelengths is natural. The intensity of thermal bremsstrahlung and recombination radiation increases by more than a factor of two when the frequency decreases from $\nu = 10^{15}$ Hz to $\nu = 10^{14}$ Hz; i.e. in the transition from optical to IR frequencies. At the same time, the specific intensity of a blackbody with temperature $T > 10^4$ K decreases in the transition from $\nu = 10^{15}$ Hz to $\nu = 10^{14}$ Hz. This means that the fraction of non-thermal radiation significantly increases in the shift from the *V* to the *H* band, increasing the model brightness temperature of the hot line.
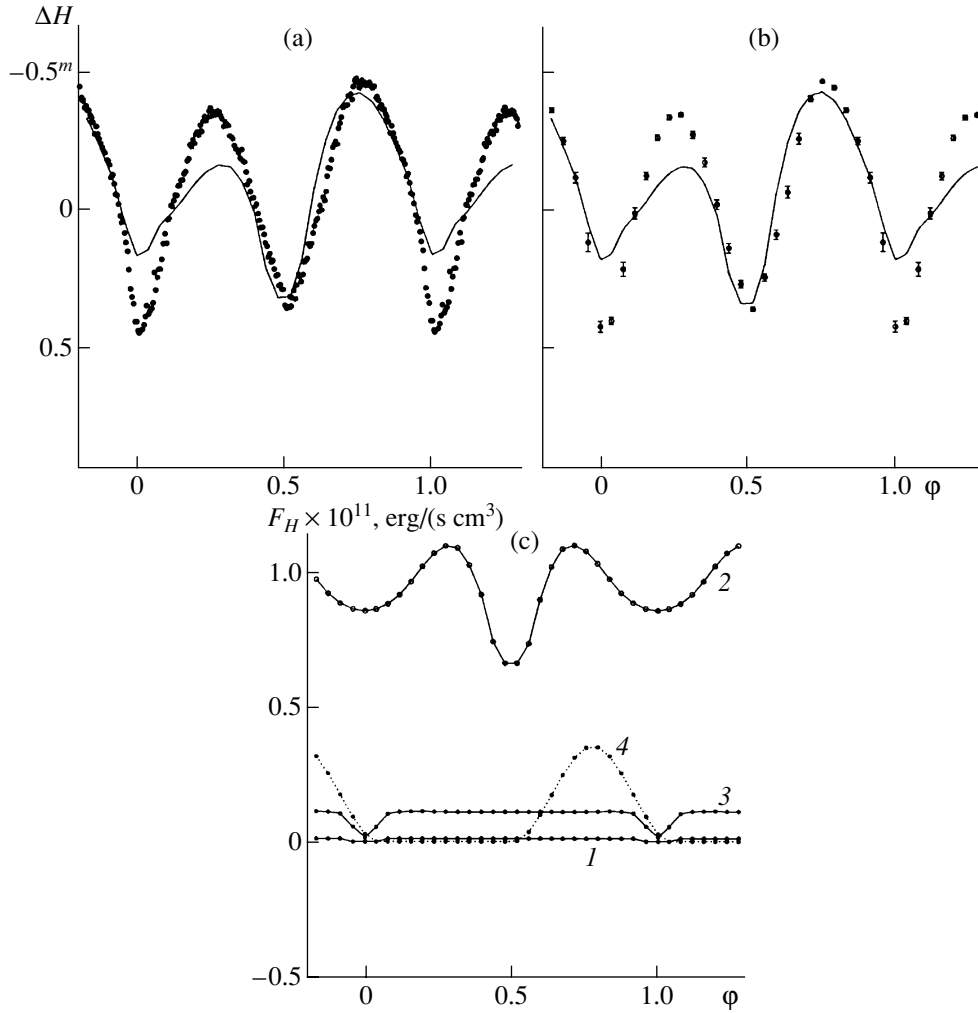
Fig. 8. IP Peg (a) observations and (b) mean light curve in the *H* filter in the inactive state. The solid curves indicate light curves synthesized with the best-fit parameters (Table 2) for the classical hot-spot model; (c) contribution of the system's components to the total radiation: (*1*) the white dwarf, (*2*) donor star, (*3*) disk, and (*4*) hot spot.

In the classical model, the allowed parameter intervals were appreciably broader than in the previous model, however we were not able to find an acceptable fit (Table 2). While the classical model provides a more or less reasonable fit for the light curve at orbital phases $\varphi \sim 0.4$–0.9, primarily due to the radiation of the hot spot (Fig. 8c), the agreement becomes quite poor at phases $\varphi \sim 0.9$–0.4 (Figs. 8a, 8b). The disk's contribution to the total flux is small ($\sim 7\%$), despite the fact that its optically thick part is very large ($R_d \sim 0.57a_0 \simeq 0.99R_{L1}$). This is consistent with the results of [18, 30]. The disk is rather cool: the brightness temperature at its outer edge is ~ 1500 K, the radial temperature distribution corresponds to $\beta_g \simeq 0.75$, the temperature of the bulk of the disk is 3500–2000 K.

In the classical model, the size of the hot spot at near-IR wavelengths ($r \sim 0.144a_0$) is roughly the same as that estimated by Froning *et al.* [30]; however, the azimuth of the spot ($\sim 80°$) is closer to that obtained at visible wavelengths (Table 2). The contribution of the spot to the total flux is $\sim 22\%$ at phases $\varphi \sim 0.75$. As in the hot-line model, the main contribution to the total flux is made by the late-type star (up to $\sim 70\%$ at $\varphi \sim 0.75$ and up to 90% at $\varphi \sim 0.25$).

7. DISCUSSION

Our interpretation of the eclipsing light curve of the cataclysmic variable IP Peg in the framework of two alternative models indicates that the hot-line model can fit the observed light curves in the quiescent state better than the hot-spot model. For example, the hot-line model provides a better fit of the widths of humps in the light curves, the shapes of eclipses, and the details of the out-of-eclipse brightness variations. This is due, in particular, to the fact that the projection onto the plane of the sky of the area of a classical hot spot with its quasi-flat surface varies rapidly during its orbital motion, resulting in the appearance of relatively narrow

humps in the eclipse light curve. In the hot-line model, the bright interaction region is an extended semi-transparent structure, whose projection onto the plane of the sky varies more smoothly with orbital phase. In addition, since the hot line supposes the de-excitation of hot plasma both forward, in the direction of orbital motion, and backward (depending on the optical depths of the interaction region and the gas stream), the hot-line model can produce broader humps in the eclipse light curve, in better agreement with the observations.

Relatively bright regions of the hot line are also observable at phases $\varphi \sim 0.5$–0.6, when a classical hot spot at the outer boundary of the disk would be invisible. Finally, if the luminosity of the hot line on the windward side exceeds that of the lateral surface of the disk, this will result in the observed increase of the flux from the system at phases $\varphi \sim 0.1$–0.2, which is completely ruled out in the classical model.

The interpretation of the IR light curves of IP Peg demonstrates convincingly the advantages of the flow model with a hot line. The residual χ^2 for the fit of the theoretical to the observed light curves for the model with a shockless interaction between the gaseous stream and the disk is 49, whereas $\chi^2 = 2681$ for the standard hot-spot model.

ACKNOWLEDGMENTS

REFERENCES

1. D. V. Bisikalo, A. A. Boyarchuk, O. A. Kuznetsov, and V. M. Chechetkin, Astron. Zh. **74**, 880 (1997) [Astron. Rep. **41**, 786 (1997)].

2. D. V. Bisikalo, A. A. Boyarchuk, O. A. Kuznetsov, and V. M. Chechetkin, Astron. Zh. **74**, 889 (1997) [Astron. Rep. **41**, 794 (1997)].

3. D. V. Bisikalo, A. A. Boyarchuk, V. M. Chechetkin, *et al.*, Mon. Not. R. Astron. Soc. **300**, 39 (1998).

4. V. G. Gorbatskiǐ, Astrofizika **3**, 245 (1967).

5. J. Smak, Acta Astron. **20**, 312 (1970).

6. M. Makita, K. Miyawaki, and T. Matsuda, Mon. Not. R. Astron. Soc. **316**, 906 (2000).

7. D. V. Bisikalo, A. A. Boyarchuk, O. A. Kuznetsov, *et al.*, Astron. Zh. **75**, 40 (1998) [Astron. Rep. **42**, 33 (1998)].

8. T. S. Khruzina, Astron. Zh. **78**, 298 (2001) [Astron. Rep. **45** (4), 255 (2001) in press].

9. B. Warner, *Cataclysmic Variable Stars* (Cambridge Univ. Press, Cambridge, 1995).

10. D. V. Bisikalo, A. A. Boyarchuk, O. A. Kuznetsov, *et al.*, Astron. Zh. **75**, 706 (1998) [Astron. Rep. **42**, 621 (1998)].

11. D. V. Bisikalo, A. A. Boyarchuk, V. M. Chechetkin, *et al.*, Astron. Zh. **76**, 905 (1999) [Astron. Rep. **43**, 797 (1999)].

12. D. V. Bisikalo, A. A. Boyarchuk, O. A. Kuznetsov, and V. M. Chechetkin, Astron. Zh. **77**, 31 (2000) [Astron. Rep. **44**, 26 (2000)].

13. T. S. Khruzina, Astron. Zh. **77**, 510 (2000) [Astron. Rep. **44**, 446 (2000)].

14. N. I. Shakura and R. A. Sunyaev, Astron. Astrophys. **24**, 337 (1973).

15. D. M. Himmelblau, *Applied Nonlinear Programming* (McGraw-Hill, New York, 1972; Mir, Moscow, 1975), p. 163.

16. V. A. Lipovetskiǐ and Dzh. A. Stepanyan, Astrofizika **17**, 573 (1981).

17. V. P. Goranskij, S. Yu. Shugarov, E. I. Orlowsky, and V. Yu. Rahimov, Inf. Bull. Var. Stars, No. 2653 (1985).

18. P. Szkody and M. Mateo, Astron. J. **92**, 483 (1986).

19. J. Wood and C. S. Crawford, Mon. Not. R. Astron. Soc. **222**, 645 (1986).

20. J. H. Wood, T. R. Marsh, E. L. Robinson, *et al.*, Mon. Not. R. Astron. Soc. **239**, 809 (1989).

21. S. Wolf, K. H. Mantel, K. Horne, *et al.*, Astron. Astrophys. **273**, 160 (1993).

22. E. T. Harlaftis, T. R. Marsh, V. S. Dhillon, and P. A. Charles, Mon. Not. R. Astron. Soc. **267**, 473 (1994).

23. A. Bobinger, K. Horne, K.-H. Mantel, and S. Wolf, Astron. Astrophys. **327**, 1023 (1997).

24. T. R. Marsh, Mon. Not. R. Astron. Soc. **231**, 1117 (1988).

25. F. V. Hessman, Astron. J. **98**, 675 (1989).

26. J. C. Martin, M. T. Friend, R. C. Smith, and D. H. P. Jones, Mon. Not. R. Astron. Soc. **240**, 519 (1989).

27. T. R. Marsh and K. Horne, Astrophys. J. **349**, 593 (1990).

28. D. Steeghs, Mon. Not. R. Astron. Soc. **281**, 626 (1996).

29. D. Steeghs, E. T. Harlaftis, and K. Horne, Mon. Not. R. Astron. Soc. **290**, L28 (1997).

30. C. S. Froning, E. L. Robinson, W. F. Welsh, and J. H. Wood, Astrophys. J. **523**, 399 (1999).

31. N. A. Webb, T. Naylor, Z. Ioannou, *et al.*, Mon. Not. R. Astron. Soc. **310**, 407 (1999).

32. P. Szkody, Astron. J. **94**, 1055 (1987).

33. S. Wolf, H. Barwig, A. Bobinger, *et al.*, Astron. Astrophys. **332**, 984 (1998).

34. K. Sawada, T. Matsuda, and I. Hachisu, Mon. Not. R. Astron. Soc. **219**, 75 (1986).

35. E. T. Harlaftis, D. Steeghs, K. Horne, *et al.*, Mon. Not. R. Astron. Soc. **306**, 348 (1999).

36. A. Bobinger, H. Barwig, H. Fiedler, *et al.*, Astron. Astrophys. **348**, 145 (1999).

37. R. Baptista, E. T. Harlaftis, and D. Steeghs, Mon. Not. R. Astron. Soc. **314**, 727 (2000).

38. L. Morales-Rueda, T. R. Marsh, and I. Billington, Mon. Not. R. Astron. Soc. **313**, 454 (2000).

39. T. S. Khruzina, Astron. Zh. **75**, 209 (1998) [Astron. Rep. **42**, 180 (1998)].

Translated by K. Maslennikov